


Interplanetary Coronal Mass Ejections Resulting from Earth-Directed CMEs Using SOHO and ACE Combined Data During Solar Cycle 23

Evangelos Paouris¹  · Helen Mavromichalaki²

Received: 27 September 2016 / Accepted: 3 January 2017 / Published online: 24 January 2017
© Springer Science+Business Media Dordrecht 2017

Abstract In this work a total of 266 interplanetary coronal mass ejections observed by the *Solar and Heliospheric Observatory/Large Angle and Spectrometric Coronagraph* (SOHO/LASCO) and then studied by *in situ* observations from *Advanced Composition Explorer* (ACE) spacecraft, are presented in a new catalog for the time interval 1996–2009 covering Solar Cycle 23. Specifically, we determine the characteristics of the CME which is responsible for the upcoming ICME and the associated solar flare, the initial/background solar wind plasma and magnetic field conditions before the arrival of the CME, the conditions in the sheath of the ICME, the main part of the ICME, the geomagnetic conditions of the ICME's impact at Earth and finally we remark on the visual examination for each event. Interesting results revealed from this study include the high correlation coefficient values of the magnetic field B_z component against the Ap index ($r = 0.84$), as well as against the Dst index ($r = 0.80$) and of the effective acceleration against the CME linear speed ($r = 0.98$). We also identify a north–south asymmetry for X-class solar flares and an east–west asymmetry for CMEs associated with strong solar flares (magnitude $\geq M1.0$) which finally triggered intense geomagnetic storms (with $Ap \geq 179$). The majority of the geomagnetic storms are determined to be due to the ICME main part and not to the extreme conditions which dominate inside the sheath. For the intense geomagnetic storms the maximum value of the Ap index is observed almost 4 hours before the minimum Dst index. The amount of information makes this new catalog the most comprehensive ICME catalog for Solar Cycle 23.

Electronic supplementary material The online version of this article (doi:[10.1007/s11207-017-1050-2](https://doi.org/10.1007/s11207-017-1050-2)) contains supplementary material, which is available to authorized users.

✉ H. Mavromichalaki
emavromi@phys.uoa.gr

E. Paouris
evpaouris@phys.uoa.gr

¹ Department of Astrophysics, Astronomy and Mechanics, Faculty of Physics, National and Kapodistrian University of Athens, 15784, Athens, Greece

² Department of Nuclear and Particle Physics, Faculty of Physics, National and Kapodistrian University of Athens, 15784, Athens, Greece

Keywords Coronal mass ejections · Interplanetary · Magnetosphere · Geomagnetic disturbances · Solar wind · Disturbances · Magnetic fields · Interplanetary

1. Introduction

Coronal mass ejections (CMEs) are magnetized structures which are ejected from the solar upper atmosphere, with velocities ranged from a few hundreds of kilometers per second up to the rare values even above of 2500 km s^{-1} (Gopalswamy, 2004). When a CME is produced over an active region, it is very likely to have enough energy in order to propagate into the interplanetary medium. The mass and the energy of a CME range from 10^{13} g to 10^{16} g and from 10^{27} erg to 10^{33} erg , respectively (Vourlidas *et al.*, 2002; Gopalswamy, 2006). These interplanetary counterparts of CMEs which are produced at the Sun are the interplanetary CMEs (ICMEs). The arrival of these ICMEs at Earth often produces geomagnetic effects (Huttunen *et al.*, 2005) as they interact with the magnetosphere of the Earth and as a result geomagnetic storms occur (Gosling, 1993; Schwenn *et al.*, 2005; Zhang *et al.*, 2007). According to Gopalswamy, Yashiro, and Akiyama (2007) a CME has to fulfill two basic requirements in order to be characterized as geoeffective: it must be an Earth-directed CME; and it must have a southward component of its magnetic field.

ICMEs and high speed streams of solar wind emanating from coronal holes are the dominant factors in geomagnetic storms. Previous studies have shown that intense geomagnetic storms are mainly caused by ICMEs, while moderate and minor storms can be caused by both ICMEs and high speed streams of solar wind (Zhang *et al.*, 2007 and references therein). There are many ICME catalogs which contain useful information as regards these events, such as those by Jian *et al.* (2006), Richardson and Cane (2010), Gopalswamy *et al.* (2010), Mitsakou and Moussas (2014) or more recently Chi *et al.* (2016). A comprehensive list of different ICME catalogs can be found at http://solar.gmu.edu/heliophysics/index.php/The_ISEST_ICME%5CCME_Lists or the ISEST Master CME list at http://solar.gmu.edu/heliophysics/index.php/The_ISEST_Master_CME_List. These lists used data from the *Interplanetary Physics Laboratory* (Wind) and *Advanced Composition Explorer* (ACE) satellites and/or the OMNI near-Earth database, taking into account all the recorded ICME data from these databases.

It is very important for a researcher to have as much information as possible for each event in order to study any connection among the CME characteristics, the ICME parameters, the associated solar flare, the solar wind plasma or the magnetic field parameters, and the geomagnetic effects when the ICME arrives at Earth. All the above ICME lists have a combination of the previous characteristics but none of them contains all of the information. This is the main purpose of the current work.

In this work a new ICME catalog is presented for the years 1996–2009, covering Solar Cycle 23. The new perspective of this study is based on two basic principles. The first principle concerns events where the CME finally appears as an ICME and is also identified in the SOHO/LASCO list. In this way the event is defined from its source at the Sun to its arrival at the ACE orbit and finally at the Earth, with information as regards the geomagnetic effects that are caused by the ICME. This means that the new catalog contains ICMEs where the source CME is well known, contrary to other published ICME catalogs (Jian *et al.*, 2006; Richardson and Cane, 2010; Mitsakou and Moussas, 2014 *etc.*) where the principle for selection of events is their detection using ACE, Wind and/or OMNI near-Earth data. The second principle is that for first time a lot of possible information per event is presented in one complete catalog. In particular we provide solar wind plasma parameters and magnetic

field data for the background conditions before the arrival of the ICME, characteristics during the event such as the presence or not of a shock wave, information on magnetic cloud structures with magnetic field rotations, as well as information on geomagnetic effects at Earth and the possible association of the source CME with solar flares.

In Section 2 we present the identification criteria used to create this catalog and give an example of our analysis, which concerns the ICME of 6 November 2000. Section 3 describes, exactly, the content of each column of this catalog and Section 4 presents the main findings of this research, such as the statistical properties of solar wind plasma parameters and magnetic fields, their association with the phase of the solar cycle and the geomagnetic effects. This section provides results through the comparison of the observations of the SOHO/LASCO coronagraph and *in situ* observations from ACE, such as the linear speed of the CME and the transit or *in situ* velocity of the ICME. We also present an analysis of associated solar flares and geomagnetic effects for Earth-directed CMEs. This gives interesting results on the distribution of the coordinates of flares on the Sun, and on the geo-effectiveness of the Earth-directed CMEs. In the last Section 5, we present a discussion of the results of our analysis and possible extensions of this study. The new ICME catalog including the full information for the 266 selected events for the time interval 1996–2009 is provided as supplementary material in the form of a spreadsheet.

2. ICME Definition and Analysis

2.1. Data Selection

Data from the *Large Angle and Spectrometric Coronagraph* (LASCO) on-board the *Solar and Heliospheric Observatory* (SOHO) are used in order to spot potential Earth-directed CMEs. In particular, data for the CMEs are taken from the SOHO/LASCO CME catalog (http://cdaw.gsfc.nasa.gov/CME_list/). In addition, we use solar wind plasma and magnetic field data from the *Advanced Composition Explorer* (ACE) MAG-SWEPAM Level 2 64-sec averages (http://www.srl.caltech.edu/ACE/ASC/level2/lvl2DATA_MAG-SWEPAM.html) for *in situ* examination of the characteristics of each ICME. For the cases with ACE data gaps for solar wind plasma and magnetic field, data from OMNI near-Earth database are used. These data obtained from OMNI are shown in red in the ICME spreadsheet. Data for solar flares are obtained from the *National Oceanic and Atmospheric Administration* (NOAA) (<ftp://ftp.ngdc.noaa.gov/STP/space-weather/solar-data/solar-features/solar-flares/x-rays/goes/>). Data for the Ap geomagnetic index are from the OMNI 2 database (<http://omniweb.gsfc.nasa.gov/>) and for the Dst index are from the Kyoto University list (http://wdc.kugi.kyoto-u.ac.jp/dst_final/index.html). Data for the aphelion and perihelion of the Earth are from the NASA/JPL DE405 astronomical ephemerides (<ftp://ssd.jpl.nasa.gov/pub/eph/planets/>).

2.2. Identification of ICMEs

Referring to previous works (*e.g.* Richardson and Cane, 2010; Mitsakou and Moussas, 2014 and references therein), ICMEs can be identified by many criteria, although a universal ICME signature is not yet determined. However, typical signatures of ICMEs such as magnetic field strength, solar wind speed, proton density, proton temperature, alpha particles to proton (He/proton) ratio, rotations of the magnetic field, and calculated plasma β are applied in this work to identify the ICME start/end time and the presence or not of the shock. Each

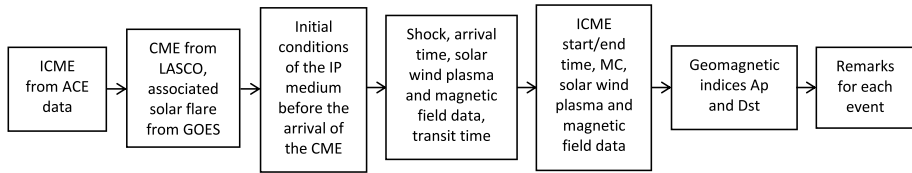


Figure 1 Flow chart of the information provided for each event in this catalog.

ICME candidate is different from any other but a combination of the previous criteria helps to identify the arrival and the boundaries of the ICME. A useful flow chart of the ICME catalogue applied to this work presenting the main parts of this list is illustrated in Figure 1.

This work presents a further investigation of the site from which the CME emerged, the solar-flare connection or not, and the geomagnetic effects caused by the ICME reaction with the Earth’s magnetosphere. The CMEs with linear speed higher than the solar wind speed create shocks in the interplanetary medium. These shocks are identified by *in situ* observations of a sudden rise of magnetic field, plasma velocity, and proton temperature and proton density. The area between the shock and the main part of the ICME is usually called the “sheath”, although it is possible that an ICME has a sheath without a shock. The solar wind is compressed in the sheath and as a result the magnetic field is increased. These large amplitude fluctuations on the magnetic field often produce high negative values of the z component of the magnetic field (B_z) which cause strong effects on the Earth’s magnetosphere (Tsurutani and Gonzalez, 1997). As an example of the identifying method, the solar wind plasma and magnetic field data from ACE for the ICME of 6 November 2000 are illustrated in Figure 2. This figure presents, from the top to bottom: a) the magnetic field magnitude (black line) with the B_z component (red line), in the Geocentric Solar Ecliptic (GSE) coordinate system, in nT; b) the solar wind velocity in km s^{-1} ; c) the latitude angle from -90 to $+90$ degrees in the Radial Tangential Normal (RTN) coordinate system; d) the longitude angle from 0 to 360 degrees in the RTN coordinate system; e) the proton density in cm^{-3} ; f) the proton temperature in K and g) the calculated plasma β . The vertical lines 1 and 2 are the boundaries of the sheath. The vertical lines 2 and 4 are the boundaries of the ICME at 6 November 2000, 22:10 UT and 8 November 2000, 02:40 UT, respectively. The arrival of the shock coincides with the first vertical line 1 at 6 November 2000, 09:15 UT, which is in accordance with the ACE shock list (http://www.ssg.sr.unh.edu/mag/ace/ACElists/obs_list.html#shocks). It is obvious that in the sheath area all of the examined signatures are at much higher levels in contrast with the main ICME part. The vertical lines 2 and 3 are the boundaries of the magnetic cloud (MC) structure. It is clear in Figure 2c that there is smooth magnetic field rotation of the θ angle from -60° to almost $+90^\circ$ while at the same time the angle φ is constant at $\approx 270^\circ$ (Figure 2d). This magnetic cloud is a part of the entire ICME and is reported also in Huttunen *et al.* (2005). For each ICME candidate signatures from the solar wind plasma and magnetic field data are visually examined, as presented in Figure 2. It is clear that the signatures for the selection of this ICME of 6 November 2000 are the low plasma β , the low proton temperature and the high He/proton ratio with the rise of the magnetic field strength and the increased solar wind velocity. This ICME is the interplanetary counterpart of the halo CME observed by the LASCO coronagraphs on the SOHO spacecraft at 18:26 UT on 3 November 2000 and is related to a C3.2 solar flare which peaked at 19:02 UT and occurred in AR9213 with coordinates N02W02. The transit velocity of the ICME’s shock at the ACE orbit is 649.1 km s^{-1} . A G2 geomagnetic storm triggered by the sheath of the ICME occurred on

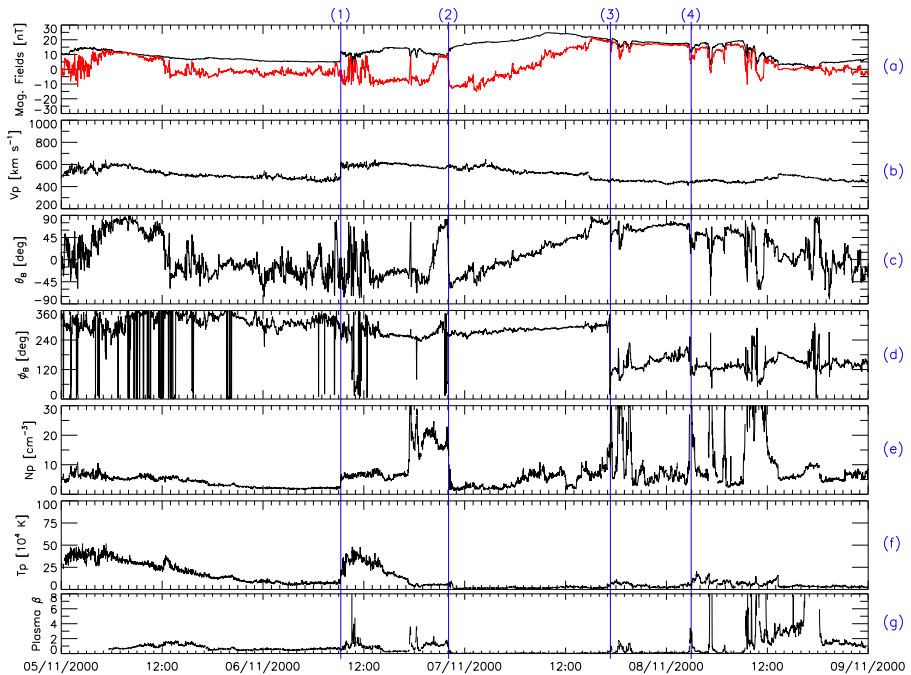


Figure 2 Example of an ICME on 6 November 2000. From top to the bottom are the magnetic field and solar wind plasma data from ACE in the GSE coordinate system, showing in a) the magnetic field strength (black line) with the B_z component (red line) in nT, b) solar wind velocity in km s^{-1} , c) the latitude angle from -90 to $+90$ degrees in the RTN coordinate system, d) the longitude angle from 0 to 360 degrees in the RTN coordinate system, e) the proton density in cm^{-3} , f) the proton temperature in K, and g) the calculated plasma β . The first vertical blue line 1 indicates the arrival time of the ICME-driven shock. The region between 1 and 2 is mentioned as the sheath of the ICME. The next two vertical lines 2 and 3 indicate the magnetic cloud structure which in c) shows a smooth rotation in B , and finally the vertical lines 2 and 4 indicate the boundaries of the ICME, *i.e.* the starting and ending times.

6 November 2000, with a Dst index minimum equal to -159 nT at 21:00–22:00 UT and an Ap maximum (3-hour interval) equal to 132 from 18:00 to 21:00 UT.

2.3. Calculations from ACE and SOHO Data

2.3.1. Plasma β

As the plasma β is one of the signatures of the examined ICME events and as the ACE data do not contain values of this parameter, we calculate them from other known variables such as the magnetic field strength, the proton temperature and density and the He/proton ratio. The known variables are available by the *Magnetic Field Experiment* (MAG) (Smith *et al.*, 1998) and *Solar Wind Electron, Proton, and Alpha Monitor* (SWEPAM) (McComas *et al.*, 1998) instruments. The plasma β is equal to the ratio of the gas pressure p_{gas} to magnetic pressure p_{mag} . The magnetic pressure is calculated exactly, as the magnetic field strength B is available from the magnetic field measurements by the MAG instrument, using the equation $p_{\text{mag}} = B^2/8\pi$. The gas pressure calculated using the equation $p_{\text{gas}} = p_p + p_\alpha + p_e$ where p_p , p_α and p_e are the contribution of protons, alpha particles and electrons to the

gas pressure, respectively (Mullan and Smith, 2006). The proton contribution is calculated from the equation $p_p = N_p k T_p$ directly as the proton temperature T_p and the number density of protons N_p are available from the thermal particle measurements from the SWEPM instrument. The alpha particle contribution is calculated using the equation $p_\alpha = 4R_\alpha N_p k T_p$ using the assumption that $T_\alpha = 4T_p$ (Bochsler, Geiss, and Joos, 1985) and the ratio of the number density of alpha particles to the proton number density R_α is also available from the SWEPM instrument. Finally, the electron contribution is calculated using the equation $p_e = (1 + 2R_\alpha)N_p k T_e$ using the assumption that $T_e \approx 1.41 \times 10^5$ K (Newbury *et al.*, 1998).

2.3.2. Distance of ACE Satellite from the Sun

The ACE orbit is at the L1 libration point between the Sun and the Earth at a distance of about 1/100 of 1 AU from the Earth. For this work a code has been developed which takes into account the epoch and the aphelion/perihelion of Earth in order to calculate more accurately the distance of the Earth and as a result the distance of ACE spacecraft from the Sun. This more accurate distance d is used in order to estimate the transit velocity of the CME from Sun to ACE, V_{tr} (column 21 in the catalog) using the time of the onset of the CME from LASCO t_1 (column 1) and the arrival time on ACE orbit t_2 (column 19) through the equation $V_{tr} = d/\tau$ where $\tau = (t_2 - t_1)$ is the transit time.

3. ICME Catalog Description

In Section 2 the criteria which characterize an ICME event are described and as a result a total of 266 ICMEs are identified. These ICMEs are presented with full details in the electronic supplementary material, as a spreadsheet.

In columns 1–4 of the spreadsheet the characteristics for the most probably associated CME from the SOHO/LASCO list are given. Specifically, column 1 gives the date and time corresponded to the first observation of the related CME by the LASCO coronagraphs on the SOHO spacecraft, and column 2 shows the extrapolated time of the beginning of the CME on the Sun by fitting a straight line to the height – time measurements. This time in column 1 is used to find the most probable associated solar flare. Specifically, for the cases where the time in column 2 is earlier than the time in column 1, a time window ± 1 hour of the time in column 2 is used for estimating the most probable solar flare. In addition, a further study taking into account the active region coordinates of the flare, aiming to provide more information, is performed. If the time in column 2 is after the time in column 1, then the time in column 1 has taken into account the time window of ± 1 hour in order to estimate the most probable time of the solar flare. Column 3 shows the angular width and column 4 shows the linear speed of the CME.

Columns 5–8 show information as regards the solar flare related to the CME in column 1. Specifically, column 5 shows the solar-flare class, column 6 the peak time of the solar flare, column 7 the active region and column 8 the exact coordinates of the solar flare where possible, or the coordinates of the active region on the surface of the Sun. If there is not a possible associated solar flare a “no flare” label is presented in column 5, and the columns 6–8 are intentionally filled with a dash.

Columns 9–17 present the initial/background conditions of the interplanetary (IP) medium at ACE’s orbit before the arrival of the ICME, such as the mean solar wind plasma and the magnetic field values. Columns 9 and 10 are the time window for the examination of the background conditions before the arrival of the shock or the ICME. Columns 11–17

give the mean values of the speed of the solar wind, the magnetic field, the B_z component of the magnetic field, the proton temperature, the proton density, the He/proton ratio and plasma β , respectively.

Columns 18 to 32 are relative to information as regards the sheath of the ICME. The symbols 1 and 0 used in column 18 indicate that the ICME had or did not have an ICME-driven shock, respectively. Column 19 shows the disturbance time, especially for the fast ICMEs. This column gives the time in UT of the arrival of the ICME-driven shock. The time of the arrival of the shock from the ACE list as mentioned in the previous section is also given in parentheses. If there is no discontinuity in the case without a shock, as happens when the ICME velocity and the magnetic field are similar to the ambient solar wind, then the disturbance time corresponds to the start time of the ICME which is shown in column 33. Column 20 represents the transit time of the CME from the Sun to the ACE orbit. Column 21 shows the shock transit speed at the ACE orbit as described in Section 2.3.2. Column 22 is the effective acceleration (see Section 4.5). Columns 23–32 give the mean value of the speed of the solar wind, the maximum speed of the solar wind, the mean magnetic field, the maximum value of the magnetic field, the mean B_z component of the magnetic field, the minimum value of B_z component, the mean proton temperature, the mean proton density, the mean He/proton ratio and the mean plasma β , respectively.

Columns 33–46 relate to information as regards the main part of ICME. Columns 33 and 34 give the ICME start time as well the end time, respectively. Column 35 indicates that the ICME includes or not a magnetic cloud. There are three cases: the symbol 2 indicates the existence of a magnetic cloud (Burlaga *et al.*, 1981), the symbol 1 is used for those cases in which evidence of a rotation of the magnetic field exists but overall the magnetic field characteristics do not meet those of a magnetic cloud (Richardson and Cane, 2010), and finally, the symbol 0 is used for events with no magnetic cloud-like magnetic field features. Columns 36–38 give the mean plasma velocity of the ICME, the maximum velocity of the ICME, the difference between the speed of the solar wind before the ICME (taken from column 11) and the velocity of the ICME (taken from column 36), respectively. Columns 39–46 present the mean and the maximum values of the magnetic field, the mean and minimum B_z component values, the mean proton temperature of the ICME, the mean proton density, the mean He/proton ratio and the mean plasma β , respectively.

Columns 47–50 give information as regards the geomagnetic conditions which are caused by the arrival of the ICME and the interaction with the Earth's magnetosphere. Column 47 gives the Dst index minimum value and column 48 shows the date and the time when this value is reported. Column 49 shows the geomagnetic Ap index maximum value and column 50 shows the 3-hour interval when the previous value was reported.

Finally, column 51 contains a brief comment on the visual examination of the signatures of the ICME which are described in Section 2.2.

4. Properties of ICMEs

4.1. Solar Wind Plasma Parameters and Magnetic Field Values

For each examined case we calculate the mean values of the magnetic-field magnitude, the southward component of magnetic field, the velocity, the proton density, the proton temperature, the plasma β , and the He/proton ratio for the time interval before the arrival of the ICME-driven shock and during the sheath and the ICME.

The statistical analysis reveals that the magnetic field before the arrival of the ICME (initial/background conditions) is $B_{\text{init}} = 6.73 \pm 0.19$ nT (the standard error is on the mean of all events), and the southward B_z component is $B_{z_init} = -0.13 \pm 0.21$ nT. The mean velocity is $V_{\text{init}} = 421.8 \pm 5.7$ km s⁻¹. The means of proton density, proton temperature, plasma β and alpha ratio for the period before the arrival of the ICME are $N_{p_init} = 6.84 \pm 0.29$ cm⁻³, $T_{p_init} = (7.85 \pm 0.69) \times 10^4$ K, $\beta_{\text{init}} = 1.68 \pm 0.10$, and $R_{\alpha_init} = 0.042 \pm 0.002$, respectively. These values are typical solar wind plasma values.

For the sheaths (disturbed conditions) the values of magnetic field are $B_{\text{dist}} = 12.66 \pm 0.39$ nT and $B_{z_dist} = 0.06 \pm 0.28$ nT, respectively. The mean velocity is $V_{\text{dist}} = 513.3 \pm 8.5$ km s⁻¹. The solar wind plasma values are $N_{p_dist} = 14.36 \pm 0.60$ cm⁻³, $T_{p_dist} = (1.78 \pm 0.98) \times 10^5$ K, $\beta_{\text{dist}} = 1.85 \pm 0.13$, and $R_{\alpha_dist} = 0.036 \pm 0.002$, respectively. These values are much higher than typical solar wind values as a result of the conditions inside the sheaths, where the magnetic field is compressed leading to higher values of magnetic field, velocity, proton density and proton temperature.

The mean magnetic field components for the ICMEs are $B_{\text{ICME}} = 10.38 \pm 0.29$ nT and $B_{z_ICME} = -0.30 \pm 0.28$ nT. The solar wind plasma means are $V_{\text{ICME}} = 483.2 \pm 6.9$ km s⁻¹, $N_{p_ICME} = 6.99 \pm 0.27$ cm⁻³, $T_{p_ICME} = (7.41 \pm 0.39) \times 10^4$ K, $\beta_{\text{ICME}} = 0.84 \pm 0.05$, and $R_{\alpha_ICME} = 0.049 \pm 0.003$, respectively.

The mean velocity during the sheath (V_{dist}) and/or the ICME (V_{ICME}) is higher than the velocity of the ambient solar wind (V_{init}) indicating expansion of CMEs into the interplanetary medium.

It is noteworthy that inside the ICME the southward component of the magnetic field B_z , the proton density and the proton temperature are at very low levels relative to the background conditions or typical interplanetary medium values. In particular, the plasma β is much lower than in sheaths and while $\beta < 1$ the magnetic pressure is the dominant factor inside the ICMEs. Furthermore, the He/proton ratio of ICMEs (R_{α_ICME}) is higher than in sheaths or the typical solar wind values, as it has been well established for many years that some ICMEs are associated with high values of the He/proton ratio (Borriani *et al.*, 1982). The solar wind He/proton ratio, as mentioned in Section 2.2, is not a prime identifier but one of the signatures which is used in combination with other signatures for ICME identification. The reasons the He/proton ratio is not a prime identifier are also found in Richardson and Cane (2010). The magnetic field values are at higher levels than in typical solar wind values ($B_{\text{ICME}} > B_{\text{init}}$) and very close to the values inside the sheath. The southward component in ICMEs is lower than even the sheath ($B_{z_ICME} < B_{z_dist}$) and that is a very interesting find which indicates that the majority of the geomagnetic storms are due to the main part of the ICME and not to the sheath while the magnetic field strength and velocity are at the higher levels $B_{\text{dist}} > B_{\text{ICME}}$ and $V_{\text{dist}} > V_{\text{ICME}}$, respectively. All the above information is presented in Table 1. The mean angular width of CMEs it was found to be $272.3^\circ \pm 6.6^\circ$. The majority of events (55.6 %) are halo CMEs. If the 148 halo CME events (with angular width equal to 360°) are excluded from the total number of CMEs, then the mean angular width is $161.7^\circ \pm 6.0^\circ$. A width distribution for the examined events is presented in Figure 3 (top panel).

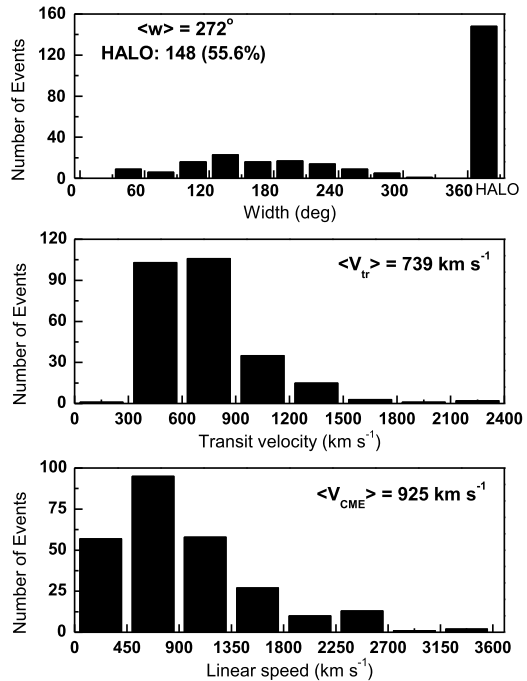
4.2. ICME Transit Velocity and CME Linear Speed

For the examined events the transit velocity of each ICME is calculated and it is found to range from 296.4 km s⁻¹ up to 2212.8 km s⁻¹ with a mean value of 739.1 ± 18.1 km s⁻¹, which is almost 71 % higher than the mean solar wind speed. The mean solar wind speed is calculated from the initial/background conditions (column 8) and is found to be

Table 1 Mean values of the solar wind plasma and magnetic field data for the conditions before the arrival of the ICME-driven shock, the sheath and the ICME.

Parameter	Initial conditions	Sheath	ICME
Magnetic field strength B [nT]	6.73 ± 0.19	12.66 ± 0.39	10.38 ± 0.29
Southward component B_z [nT]	-0.13 ± 0.21	0.06 ± 0.28	-0.30 ± 0.28
Velocity V [km s^{-1}]	421.8 ± 5.7	513.3 ± 8.5	483.2 ± 6.9
Proton density N_p [cm^{-3}]	6.84 ± 0.29	14.36 ± 0.60	6.99 ± 0.27
Proton temperature T_p [K]	$(7.85 \pm 0.69) \times 10^4$	$(1.78 \pm 0.98) \times 10^5$	$(7.41 \pm 0.39) \times 10^4$
Plasma β	1.68 ± 0.10	1.85 ± 0.13	0.84 ± 0.05
He/proton ratio R_α	0.042 ± 0.002	0.036 ± 0.002	0.049 ± 0.003

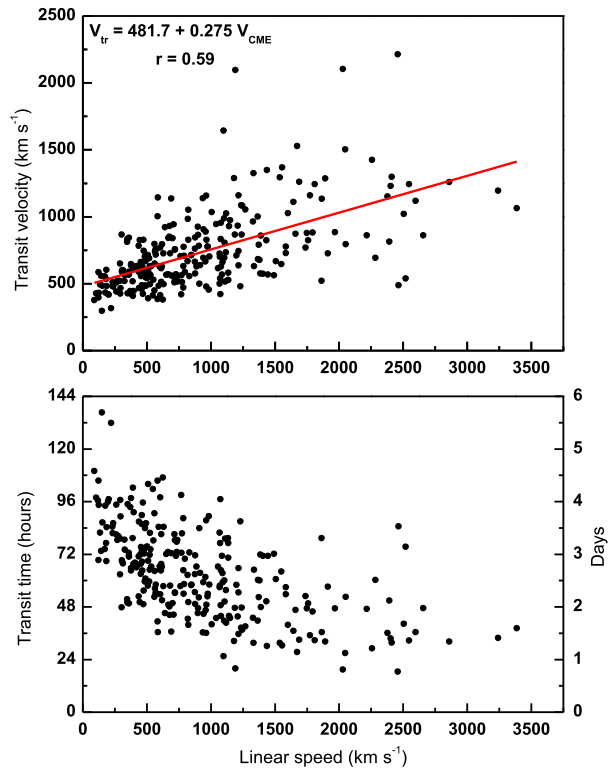
Figure 3 Angular width (w), transit velocity (V_{tr}), and CME linear speed (V_{CME}) distributions of examined events. The bin size for the width distribution is 30° , for the transit velocity is 300 km s^{-1} and for the CME linear speed is 450 km s^{-1} .



421.8 km s^{-1} . A distribution of the transit velocity of the examined events is presented in Figure 3 (middle panel). The CME linear speed ranges from 91 km s^{-1} up to 3387 km s^{-1} with a mean value of $924.5 \pm 38.8 \text{ km s}^{-1}$. A distribution of CME linear speed for the examined events is presented in Figure 3 (bottom panel).

The transit velocity and the CME linear speed from SOHO/LASCO are described by the relation $V_{tr} = a + bV_{CME}$ (in km s^{-1}) in which $a = 481.7 \pm 26.0 \text{ km s}^{-1}$ and $b = 0.275 \pm 0.023$. The CME linear speed calculated by SOHO/LASCO is projected against the plane of the sky and does not represent the true Earthward-directed speed of the CME, although it is possible to have some degree of correlation (Cane, Richardson, and St. Cyr, 2000). The cross correlation coefficient of the above examined events is $r = 0.59$. The fastest disturbance transit speed for a given CME speed is given by $V_{tr} = 431 + 0.73V_{CME}$ (in km s^{-1}), slightly different from the relation of Richardson and Cane (2010). This relation was suggested by

Figure 4 The transit velocity with respect to the linear speed of the CME plane of the sky expansion observed by LASCO (top panel) and disturbance transit time with respect to the linear speed of the CME (bottom panel).



Richardson and Cane (2010) for use to forecast the earliest time that the influence of an Earth-directed CME is experienced in the near-Earth solar wind.

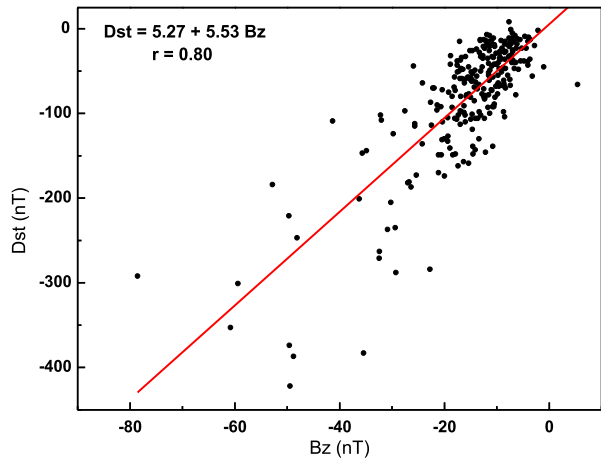
Figure 4 presents the transit velocity of the disturbance against the linear speed of the CME (upper panel) and the disturbance transit time against the CME linear speed (bottom panel). The transit time of the examined events ranges from 18.5 hours (≈ 0.8 days) up to 136.6 hours (≈ 5.7 days) with a mean value of 62.9 hours (≈ 2.6 days).

4.3. Dst-Index Minimum and B_z Component

The Dst index is a measure of the strength of the ring current and is the commonly used index to estimate the intensity of geomagnetic storms. This index takes positive (up to $\approx +50$ nT) and negative values (up to ≈ -400 nT). The positive values are mostly caused by the compression of the magnetosphere from solar wind pressure increases. The negative values are associated with disturbances, due to CMEs and/or high speed streams of solar wind, at the ring current producing geomagnetic storms. Many researchers define intense geomagnetic storms by a value of Dst below -100 nT (Zhang *et al.*, 2007; Echer *et al.*, 2008).

The Dst index for the examined events ranges from -422 nT up to $+8$ nT with a mean Dst index value of -79.0 ± 4.4 nT. The minimum value of the southward component of the magnetic field B_z in the sheath or in the ICME ranges from -78.56 nT up to $+5.41$ nT with a mean value of -15.23 nT. The minimum value of the southward component of the magnetic field shows a very good correlation to the Dst minimum value with correlation

Figure 5 The Dst index minimum against the minimum value of the southward component of the magnetic field B_z . The red line is the linear fit of the two variables with $r = 0.80$.



coefficient $r = 0.80$. The best fit is given by the relation $Dst = a + bB_z$, where $a = 5.27 \pm 4.69$ nT and $b = 5.53 \pm 0.25$ (Figure 5).

We note that the correlation between the Dst minimum and the velocity V_{max} in the sheath or in the ICME is calculated to be $r = 0.39$, which means the B_z component is better correlated with the Dst index than the velocity. Therefore the magnetic field in the sheath or the ICME plays the most important role in the creation of geomagnetic storms. This would be a good tool for forecasting studies.

4.4. Ap Index and B_z Component

The levels of geomagnetic activity are determined mainly by two indices, the Kp and Ap indices. The Ap geomagnetic index is a planetary index as it is an average over the globe, in contrast with the Kp index, which is the mean standardized from 13 geomagnetic observatories. The values of the Ap index range from 0 to 400. As a global index, Ap is the most important index for forecasting geomagnetic conditions, and is the only global magnetic index predicted by the space weather forecasting centers (McPherron, 1999; Mavromichalaki *et al.*, 2015).

The mean value of the Ap index based on the maximum 3-hour interval of the examined events is calculated to 85.0 ± 4.5 with values ranging from 6 up to 400 over the 266 events. The minimum B_z value (in the sheath or in the ICME) and the Ap-index maximum values are highly correlated, with $r = 0.84$ under the expression $Ap = a + bB_z$, with $a = -10.13 \pm 4.63$ and $b = -6.25 \pm 0.25$, where B_z is in units of nT. The Ap values are plotted against the minimum B_z in Figure 6. It is well established by previous researchers (Gopalswamy, 2009; Tsurutani and Gonzalez, 1997) that the intensity of the resulting magnetic storm depends on the magnitude of the southward magnetic field component B_z . Our result that the Ap index correlates better than the transit velocity indicates that Ap should be the dominant forecasting variable for space weather studies. This has been already applied at the Athens Space Weather Forecasting Center (ASWFC) where a daily report with a 3-day forecasting of the geomagnetic conditions and the values of Ap index is provided (Mavromichalaki *et al.*, 2015).

Figure 6 The A_p index (3-hour interval) maximum against the minimum value of the southward component of the magnetic field B_z . The red line corresponds to a linear fit which has the correlation $r = 0.84$.

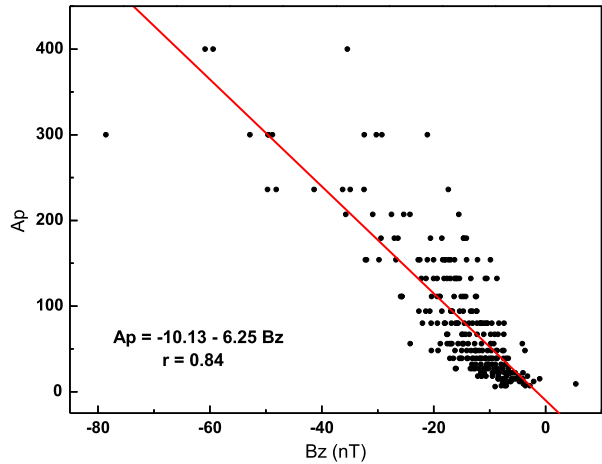
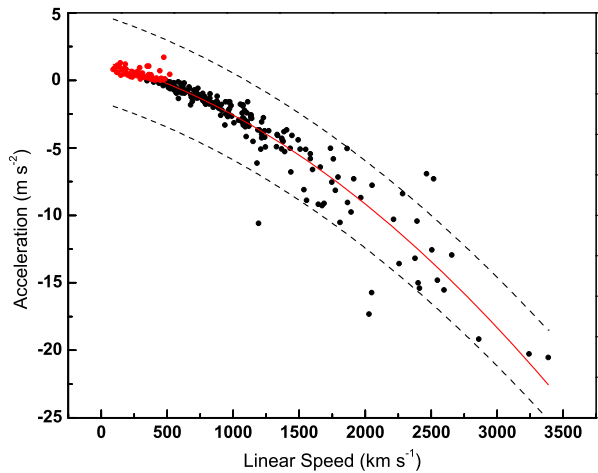


Figure 7 Scatter plot of the effective acceleration against the CME linear speed (plane of the sky expansion). The solid line is a second order polynomial fit with $r = 0.98$ in the case where the five points which are outside of the 99 % prediction levels (black dashed lines) are excluded. The effective acceleration for the slower CMEs (red color with $\alpha > 0$) is positive and for the fast CMEs (black color with $\alpha < 0$) is in general negative.



4.5. Effective Acceleration

Gopalswamy *et al.* (2000) suggested an empirical model for the arrival time of the interplanetary ejecta (IP) as a result of a study of 28 events. They used the white light CME speed as initial speed (u) and the IP ejecta speed measured at 1 AU as final speed (v). The effective acceleration α was given by $\alpha = (v - u)/\tau$, where τ was the measured transit time. The acceleration with the initial speed was fitted well to a straight line with the expression $\alpha = 1.41 - 0.0035u$, where α is in ms^{-2} , u is in km s^{-1} , and the correlation coefficient was found to be 0.98.

In our case, the linear speed of the CME from LASCO (column 4), the ICME speed (column 36), and the transit time (column 20) from our catalogue have been used to calculate the effective acceleration for each of the selected 266 events. From the scatter plot of the effective acceleration as a function of the initial speed (Figure 7), it is obvious that the best fit is a polynomial. In our case the linear fit gives a relation $\alpha = 2.918 - 0.006u$ with α in ms^{-2} and u in km s^{-1} , with a cross correlation coefficient of $r = 0.94$. This linear fit for $\alpha = 0$ implies a critical speed $u_c = 486 \text{ km s}^{-1}$, which is

higher than the typical solar wind speed as it measured from the initial/background conditions $V_{\text{init}} = 422 \text{ km s}^{-1}$. That means CMEs with $u < u_c$ are accelerated and CMEs with $u > u_c$ are decelerated. The best fit is a second order polynomial fit with the expression $\alpha = 1.62 [\text{m s}^{-2}] - 32.10 \times 10^{-4} [10^{-3} \text{ s}^{-1}] u - 1.10 \times 10^{-6} [10^{-6} \text{ m}^{-1}] u^2$, where α is expressed in m s^{-2} , u in km s^{-1} , with a cross correlation coefficient $r = 0.95$. This value is the result of applying 99 % upper and lower prediction levels. In this case only five points are outside of these borders (black dashed lines in Figure 7), and in particular three have very large values of effective acceleration (-17.3 m s^{-2} , -15.7 m s^{-2} , -10.6 m s^{-2}) and the other two had very large velocities (2465 km s^{-1} , 2519 km s^{-1}). If we exclude these five events from our sample, the correlation coefficient rises to the very high value of $r = 0.98$ with the expression $\alpha = 1.45 [\text{m s}^{-2}] - 27.40 \times 10^{-4} [10^{-3} \text{ s}^{-1}] u - 1.28 \times 10^{-6} [10^{-6} \text{ m}^{-1}] u^2$. Figure 7 confirms that the slower CMEs (red color for CMEs with $\alpha > 0$) have positive acceleration, and the faster CMEs (black color for CMEs with $\alpha < 0$) have negative acceleration, and are decelerated in general (Gopalswamy *et al.*, 2000).

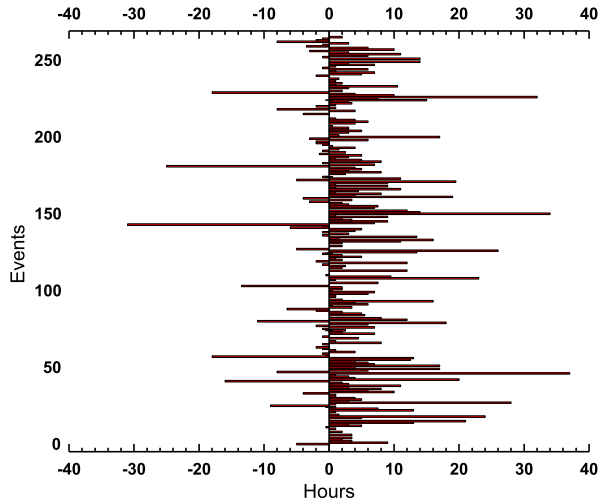
4.6. Ap Maximum and Dst Minimum

As mentioned in Section 3, columns 47–50 give information as regards the geomagnetic conditions which are caused by the arrival of the ICME and as a result the interaction with the Earth's magnetosphere. Additionally, an investigation regarding the date and time of the Dst index minimum recorded (column 48) and the date and time of the maximum 3-hour interval of the geomagnetic Ap index (column 50) has been done. The difference between the time of Dst minimum t_{Dst} and Ap maximum t_{Ap} has been calculated for each one of the 266 events through the relation $\Delta T = t_{\text{Dst}} - t_{\text{Ap}}$. Obviously $\Delta T < 0$ means that the Dst minimum value occurs before the Ap maximum value and *vice versa* for $\Delta T > 0$. This analysis reveals that in 185 events the Ap maximum value is identified before the Dst minimum value. This result is in accordance with a previous one presented by Loewe and Prölss (1997), who studied more than 1000 storms with $\text{Dst} < -30 \text{ nT}$ in the period 1953–1997 and showed that the maximum Ap and AE values precede the Dst minimum value by 1 to 2 hours. Furthermore, we find that only in 54 events the Dst minimum is identified before the Ap maximum value, and in 27 events the Ap maximum and Dst minimum are spotted almost simultaneously. These results are presented in Figure 8. We note that, for the quiet events without any geomagnetic storm consequences with $6 \leq \text{Ap} \leq 32$, in a total of 80 events, 26 events (33 %) have $\Delta T < 0$ and for the very strong geomagnetic storms with $179 \leq \text{Ap} \leq 400$, in a total of 33 events, only 7 (21 %) have $\Delta T < 0$ and the Ap maximum is noticed almost 4 hours before the Dst minimum. The mean values of these 33 events for Ap maximum is 249 and for Dst minimum is -209 nT . These results should be very helpful as a tool for space weather studies and especially for near real-time forecasting of the geomagnetic conditions. For the cases where the Dst minimum was noticed before the Ap maximum there were not recorded intense geomagnetic effects. For these events the mean values of Dst and Ap are equal to -28 nT and 21, respectively. We note that almost half of these events were observed in the declining phase of Solar Cycle 23 or during the extended solar minimum (2005–2009).

Furthermore, we note that the majority of the geomagnetic storms is due to the ICME main part and not due to the sheath. This result is strengthened from the examination of the recorded times of Dst minimum (column 48) and Ap maximum (column 50) in relation to the time of the disturbance (column 19) and the ICME start time (column 33).

In 176 events the Dst minimum is recorded during the ICME main part and only in 90 events it is recorded during the sheath. For the Ap geomagnetic index the results are more

Figure 8 Histogram of the difference between the times of Dst minimum and Ap maximum. In the majority of these events the Ap maximum occurs before (positive hours) the Dst minimum.



balanced: in 139 events the maximum Ap is recorded during the ICME, and in 127 events during the sheaths.

4.7. Associated Solar Flares

It is well known that the largest X-class solar flares are associated with CMEs. Harrison (1995) found that the fraction of flares associated with CMEs rises from 7 % to 100 % as the class of flares rises from B-class to X-class. Wang and Zhang (2007) studied 104 X-class solar flares and concluded that 90 % were associated with CMEs, and Yashiro *et al.* (2005) also found that the fraction of solar flares with CMEs increased from 20 % for flares between C3.0 and C9.0 to 100 % for the largest X-class solar flares (greater by X3.0). Andrews (2003) also showed that the majority of M-class solar flares and all X-class flares were associated with CMEs, based on the set of events studied.

For our total of 266 CMEs, 209 events (78.6 %) are associated with solar flares, while 57 events (21.4 %) are not related. Specifically, 2 events (1 %) are associated with A-class solar flares, 13 events (6.2 %) with B-class solar flares, 79 events (37.8%) with C-class solar flares, 68 events (32.5 %) with M-class solar flares and 47 events (22.5 %) with X-class solar flares.

The largest solar flares are associated with faster and usually with wider CMEs (Yashiro *et al.*, 2005; Georgoulis, 2008). The intense polarity inversion lines of active regions are strongly connected with the largest solar flares and are statistically associated with fast CMEs (Georgoulis, 2008).

In the present study a further analysis, based on the linear speed of the CME and the transit velocity of the ICME with the associated solar flare, is performed. The mean linear speed of the events which are not associated with solar flares is 478.1 km s^{-1} while for the events which are associated with strong X-class solar flares the mean linear speed is 1758.4 km s^{-1} . As the linear speed is projected on the plane of the sky, we also calculate the mean transit velocity and find 590.6 km s^{-1} and 1058.8 km s^{-1} , for events not associated with flares, and for events associated with flares, respectively. The mean transit velocity for the slower and not solar-flare associated events, increases from 478.1 km s^{-1} to 590.6 km s^{-1} and for the fastest ones it was decreases from 1758.4 km s^{-1} to 1058.8 km s^{-1} . This result

Table 2 Fraction of solar flares (SFs) and the mean values of the linear speed of the CMEs, the transit velocity of the ICMEs, and the Dst and Ap indices.

X-ray class	Number of flares	CME linear speed [km s ⁻¹]	ICME transit velocity [km s ⁻¹]	Dst [nT]	Ap
SF	57	478.1 ± 36.3	590.6 ± 23.2	-56.9 ± 5.3	59.1 ± 6.9
A / B	15	374.5 ± 53.3	630.8 ± 62.4	-57.3 ± 7.5	52.5 ± 11.4
C	79	724.9 ± 45.0	682.8 ± 28.4	-76.8 ± 6.5	78.2 ± 7.0
M	68	1078.2 ± 56.4	731.8 ± 27.9	-83.4 ± 10.4	88.4 ± 9.6
X	47	1758.4 ± 97.9	1058.8 ± 50.2	-110.3 ± 14.0	133.3 ± 15.4

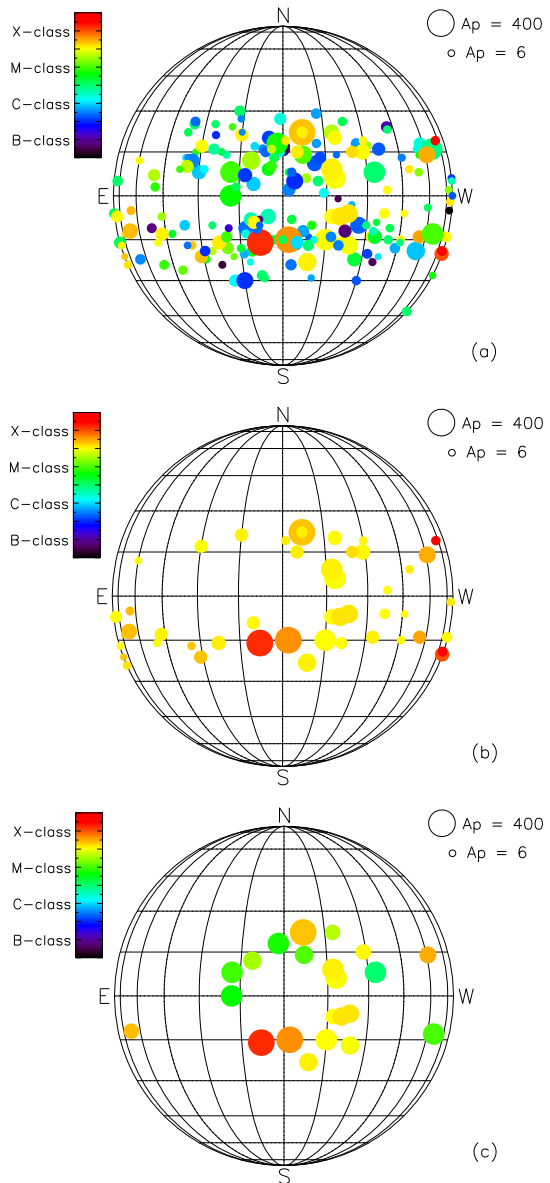
is in accordance with the results of Section 4.5 noting that the fastest events are decelerated in the interplanetary medium and the slower ones are accelerated in general. Moreover, the most energetic X-class solar flares associated with CMEs resulting in ICMEs trigger the most intense geomagnetic storms with a mean Dst minimum value of -110 nT, while the mean Ap geomagnetic index is 133. These results are summarized in Table 2. These events are located very close to the center of the Sun's visible disk as shown in Figure 9a. The size of the solar flare is indicated by color from B-class (dark blue) to X-class (red) and the size of the produced geomagnetic storm is given by the size of the circle. The smallest circle is for Ap = 6 (quiet conditions) and Ap = 400 (extreme conditions) is represented by the biggest circle.

A north-south asymmetry for the X-class solar flares is noticeable: 17 events are located in the northern hemisphere while 30 events are in the southern hemisphere (Figure 9b). If we take into account the geomagnetic effectiveness of events with flares of magnitude greater than M1.0, then we notice one more asymmetry, an east-west asymmetry, as the majority of the most intense geomagnetic storms with (Ap ≥ 179) seem to be associated with events from the western part of the visible solar disk. In particular, 6 events with Ap ≥ 179 are located in the eastern part of the visible solar disk, while 16 events are located in the western part (Figure 9c). Papailiou *et al.* (2013) showed that the helio-longitude of a solar flare associated with a cosmic ray intensity decrease is located in the 50°–70° W sector and the maximum values of the geomagnetic activity index Kp_{max} are ≥ 5 (Ap ≥ 48). From this figure it is also obvious that the M-class solar flares associated with events which produce strong geomagnetic storms are located in the northern hemisphere of the visible solar disk and only one event is in the southern hemisphere. This result is very important specifically for space weather modeling and may be used in existing models (Mavromichalaki *et al.*, 2015) as an index related to the coordinates of the associated solar flare of a CME.

4.8. Phases of Solar Cycle 23

Following previous work (Paouris *et al.*, 2012; Chowdhury, Kudela, and Dwivedi, 2013; Gushchina *et al.*, 2014), the ICME characteristics in the current catalogue are studied separately during the ascending (January 1996 to April 1999), the maximum (May 1999 to December 2002), and the descending part of Cycle 23 (January 2003 to December 2006) as well as the minimum between Solar Cycles 23 and 24 (January 2007 to December 2009). The results of this analysis for the initial/background conditions of the solar wind plasma and magnetic field data are presented in Table 3. The mean magnetic field in typical interplanetary conditions is found to be ≈ 6–7 nT except for the period of the extended minimum,

Figure 9 From top to the bottom: a) heliographic coordinates of solar flares associated with the CMEs in our catalogue. The color of the flare is relative to the class in soft X-rays and the size of the circle is relative to the produced geomagnetic storm from this CME/ICME. b) The north–south asymmetry for X-class solar flares. c) The most intense geomagnetic storms are associated with CMEs resulting in ICMEs, around the center of the visible solar disk. An east–west asymmetry is also noticed for these events.



in which it is at lower levels ($\approx 3\text{--}4$ nT) as a result of the very quiet conditions. Typical interplanetary values are identified also for proton density and temperature. The velocity, the magnetic field strength, the proton temperature and the geomagnetic indices A_p and Dst , reached their maximum values in the descending phase of the cycle. This is in accordance with previous results as Solar Cycle 23 was an interesting cycle with a lot of extreme events during this period, such as October–November 2003, January 2005 and December 2006 (Paouris *et al.*, 2012). During the whole cycle the plasma β is above unity as a result of the solar wind and magnetic field conditions in which the gas pressure is the dominant factor.

Table 3 Mean values of the initial/background solar wind plasma, magnetic field data, and geomagnetic indices for the ascending, maximum, and descending phases of Solar Cycle 23.

Parameter	Ascending phase 1/1996–4/1999	Solar maximum 5/1999–12/2002	Descending phase 1/2003–12/2006	Extended minimum 1/2007–12/2009
Magnetic field strength B [nT]	6.32 ± 0.46	6.79 ± 0.24	7.12 ± 0.39	3.50 ± 0.47
Southward component B_z [nT]	-0.03 ± 0.43	-0.16 ± 0.27	-0.10 ± 0.50	-0.23 ± 0.71
Velocity V [km s^{-1}]	376.8 ± 9.9	410.3 ± 6.9	477.8 ± 12.1	360.5 ± 32.2
Proton density N_p [cm^{-3}]	9.53 ± 0.70	6.54 ± 0.38	5.70 ± 0.51	6.37 ± 1.32
Proton temperature T_p [K]	$(6.26 \pm 0.83) \times 10^4$	$(8.18 \pm 1.19) \times 10^4$	$(8.58 \pm 0.95) \times 10^4$	$(3.49 \pm 0.43) \times 10^4$
Plasma β	2.56 ± 0.31	1.48 ± 0.12	1.48 ± 0.15	6.50 ± 4.08
He/proton ratio R_α	0.028 ± 0.004	0.046 ± 0.003	0.044 ± 0.004	0.017 ± 0.004
A_p	69.9 ± 8.3	81.4 ± 6.0	106.7 ± 11.1	19.5 ± 7.4
Dst [nT]	-68.2 ± 6.0	-78.2 ± 5.9	-92.0 ± 10.1	-20.3 ± 4.0

Table 4 Mean values in the sheaths for solar wind plasma parameters, magnetic field data, and geomagnetic indices for the different phases of the Solar Cycle 23 and the minimum between Solar Cycles 23/24.

Parameter	Ascending phase 1/1996–4/1999	Solar maximum 5/1999–12/2002	Descending phase 1/2003–12/2006	Extended minimum 1/2007–12/2009
Magnetic field strength B [nT]	11.24 ± 0.71	12.96 ± 0.52	13.54 ± 0.87	5.65 ± 0.71
Southward component B_z [nT]	$+0.32 \pm 0.65$	$+0.12 \pm 0.34$	-0.29 ± 0.64	$+0.95 \pm 0.74$
Velocity V [km s^{-1}]	438.6 ± 12.5	504.3 ± 9.9	587.4 ± 19.5	392.4 ± 25.3
Proton density N_p [cm^{-3}]	17.97 ± 1.43	14.32 ± 0.79	12.21 ± 1.23	13.65 ± 2.74
Proton temperature T_p [K]	$(1.10 \pm 0.12) \times 10^5$	$(1.95 \pm 0.20) \times 10^5$	$(2.64 \pm 0.32) \times 10^5$	$(4.89 \pm 0.34) \times 10^4$
Plasma β	2.50 ± 0.58	1.69 ± 0.14	1.60 ± 0.16	3.61 ± 0.14
He/proton ratio R_α	0.026 ± 0.002	0.037 ± 0.002	0.044 ± 0.004	0.018 ± 0.005
A_p	69.9 ± 8.3	81.4 ± 6.0	106.7 ± 11.1	19.5 ± 7.4
Dst [nT]	-68.2 ± 6.0	-78.2 ± 5.9	-92.0 ± 10.1	-20.3 ± 4.0

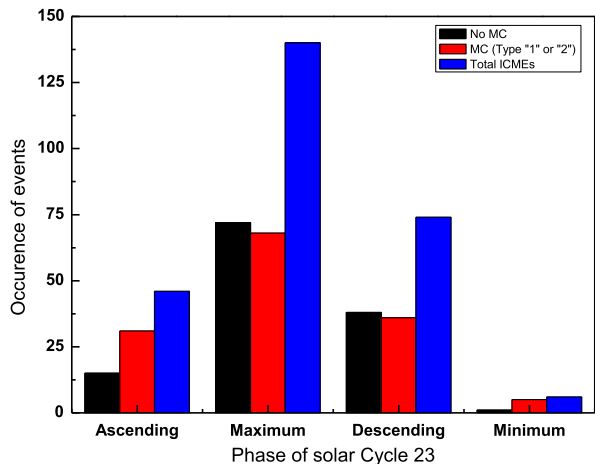
The results concerning the disturbed conditions during the phases of Solar Cycle 23 are presented in Table 4. As expected all the variables show an increase as a result of the conditions inside the sheath, where the magnetic field is compressed, leading to higher values of the magnetic field, velocity, proton density and proton temperature. The maximum values for most of the variables occur in the descending phase of the cycle, as explained above.

Finally, Table 5 gives the results during the ICME as a function of the phases of the solar cycle. It is noteworthy that the magnetic field and the solar wind speed inside the ICME are higher than typical solar wind values, but lower compared to the values inside the sheaths. The plasma β and proton temperature are at lower levels, close to the initial conditions before the arrival of the ICME-driven shock, while the He/proton ratio takes remarkable

Table 5 Mean values during the ICME of the solar wind plasma parameters, magnetic field data, and geomagnetic indices for the different phases of Solar Cycle 23 and the minimum between Solar Cycles 23/24.

Parameter	Ascending phase 1/1996–4/1999	Solar maximum 5/1999–12/2002	Descending phase 1/2003–12/2006	Extended minimum 1/2007–12/2009
Magnetic field strength B [nT]	11.26 ± 0.55	9.68 ± 0.37	11.27 ± 0.66	9.03 ± 1.86
Southward component B_z [nT]	-0.57 ± 0.81	$+0.09 \pm 0.34$	-0.74 ± 0.56	-1.71 ± 1.57
Velocity V [km s^{-1}]	427.9 ± 9.9	474.4 ± 8.7	543.3 ± 14.7	376.6 ± 21.4
Proton density N_p [cm^{-3}]	8.58 ± 0.59	6.86 ± 0.38	6.51 ± 0.58	7.04 ± 1.28
Proton temperature T_p [K]	$(6.49 \pm 0.84) \times 10^4$	$(7.33 \pm 0.63) \times 10^4$	$(9.51 \pm 0.87) \times 10^4$	$(2.17 \pm 0.31) \times 10^4$
Plasma β	0.75 ± 0.09	0.95 ± 0.08	0.78 ± 0.09	0.65 ± 0.16
He/proton ratio R_α	0.055 ± 0.011	0.048 ± 0.002	0.049 ± 0.004	0.018 ± 0.004
A_p	69.9 ± 8.3	81.4 ± 6.0	106.7 ± 11.1	19.5 ± 7.4
Dst [nT]	-68.2 ± 6.0	-78.2 ± 5.9	-92.0 ± 10.1	-20.3 ± 4.0

Figure 10 Histogram of the total number of ICMEs and the magnetic cloud fraction with respect to the phases of the Solar Cycle 23.



higher values. This is in accordance with the criteria which have been applied in this work for the identification of the ICMEs, as described in Section 2.2. In particular, the plasma β for the entire cycle remains below unity, which indicates the dominance of the magnetic pressure inside the ICMEs.

As presented in previous work (*e.g.* Richardson and Cane, 2010 and references therein), there is evidence of a solar-cycle dependence in the fraction of ICMEs that have the characteristics of magnetic clouds, with the fewer ICMEs around solar minimum having a higher incidence of MCs than ICMEs around solar maximum. In this study we find that 140 (52.6 %) events are magnetic clouds (MCs) or possible MCs (2 or 1 in column 35, respectively) and 126 events (47.4 %) are described as ICMEs without MC characteristics. A histogram of the occurrence of the examined events as a function of the phases of the solar cycle is given in Figure 10. It is notable that in the ascending phase of the cycle, 31 events

have MC characteristics, while at the solar maximum 68 events, in the descending phase 36 events, and during the extended minimum only 5 events, have MC characteristics.

4.9. Semiannual Variation of Geomagnetic Activity

It is well known that geomagnetic activity tends to be higher in the months around equinoxes than the months at the solstices (Gonzalez and Tsurutani, 1992; Crooker, Cliver, and Tsurutani, 1992). However, there is no universal accepted explanation in the scientific community for this behavior (Gonzalez, Clua de Gonzalez, and Tsurutani, 1993). The three dominant mechanisms which have been proposed for the seasonal variation of the geomagnetic activity are: 1) the equinoctial hypothesis (Bartels, 1932; McIntosh, 1959; Svalgaard, 1977), 2) the Russell–McPherron mechanism (Russell and McPherron, 1973) and 3) the axial hypothesis (Cortie, 1912). The first explanation is based on the 23° tilt of Earth's equatorial plane to the ecliptic plane and the 11° offset between Earth's rotation and dipole axes. The second is based on the 26° angle between the Sun's and Earth's equatorial planes and the 11° dipole axis offset and finally the third is based on the 7° tilt of the solar equatorial plane to the ecliptic plane.

The mean monthly values of the Ap and Dst indices for the examined events presents a clear seasonal variation, with the maximum of Ap and the minimum Dst mean values occurring in the equinoctial months March/September and the months ahead showing a time-lag after the equinoxes, April–May and October–November respectively (Figure 11, left panel). This result is in accordance with previous results from Gonzalez and Tsurutani (1992) and Crooker, Cliver, and Tsurutani (1992). Crooker, Cliver, and Tsurutani (1992) showed that the number of great storms with $Ap > 100$ in the equinoctial months (March–April and September–October) was larger than the number of large storms in the solstitial months (December–January and June–July) for the period 1932–1989, by a ratio 3:1. Gonzalez and Tsurutani (1992) showed that intense geomagnetic storms with $Dst < 100$ nT during the time interval 1975–1986 tended to occur within the solar cycle with a dual-peak distribution. The current study also confirms these results: for the examined events which produce

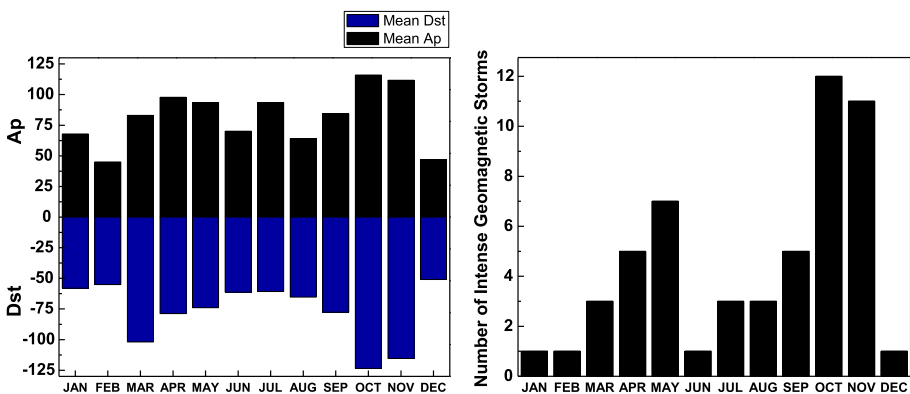


Figure 11 Histogram of the mean Ap and Dst indices per month for the examined events (left panel). The seasonal distribution of major ($Dst < -110$ nT) magnetic storms for the interval 1996–2009 (right panel). It is obvious that the higher values for Ap and the minimum for Dst respectively occur in the spring and autumn seasons with two intervals of maximum storm occurrence: March–April–May, and September–October–November. The months of minimum storm occurrences are December–January–February, and June. The months of maximum occurrence of storms are close to the solar equinoxes implying a semiannual variation of geomagnetic activity.

a geomagnetic storm with $Dst < 110$ nT a double peak distribution is found with peaks in April–May and October–November (Figure 11, right panel).

The mechanism for this semiannual variation of the geomagnetic activity is not clear, but it is a fact that should be considered for space weather forecasting.

5. Discussion and Conclusions

The current research catalogs a total of 266 ICME events including a lot of information in a table of 51 columns. These events are identified from observations by the LASCO instrument on SOHO spacecraft. *In situ* observations from ACE are used in order to define solar wind plasma and magnetic field data in three phases: before the arrival of the ICME-driven shock (referred as initial/background conditions), during the sheath (referred as discontinuity/disturbed conditions) and finally during the main part of the ICME. We note that Yermolaev *et al.* (2015) studied the temporal profiles of plasma and field parameters in the disturbed large-scale types of solar wind such as corotating interaction regions, interplanetary coronal mass ejections with magnetic clouds and/or ejecta, and sheaths and/or interplanetary shocks, adding also the background conditions before the arrival of this disturbed type of solar wind. The current work presents the first ICME catalog with a statistical analysis of the background conditions for each event. Different effects on the Earth's magnetosphere are noticed when the interplanetary medium is disturbed by multiple ICMEs, in contrast to the effects from a single ICME when the background conditions are normal. We find that, for most of the cases, if the arrival time of the shock is t_0 the background time boundaries are from $t_0 - 4$ hours to $t_0 - 1$ hours before the arrival of the shock. When multiple ICMEs occur, the time window is reduced to the period when the conditions are almost undisturbed. For the cases without a shock the time window ranges from $t_0 - 4$ hours to $t_0 - 1$ hours before the disturbed conditions of the sheath, or the main part of the ICME when the event does not appear to have a sheath (Yermolaev *et al.*, 2015).

Our catalog also presents further data including the transit time and velocity of the ICME-driven shock, the geomagnetic effects of the ICMEs on Earth's magnetosphere giving the Dst minimum and the Ap 3-hour interval maximum values, the characteristics of associated solar flares and a brief comment on the visual signatures for each event. In this way we provide as much information as possible per event.

We note that we follow a different approach for the creation of this ICME catalogue compared with existing catalogues. Past studies of Earth-directed CMEs include the following.

Jian *et al.* (2006) studied 230 ICMEs from Wind and ACE satellites for the years 1995–2004, and gave information for each event in a table of 16 columns, specifically the shock arrival time, the start and the end times of the ICME, the times for the magnetic obstacle, the peak pressure, the maximum velocities, the maximum magnetic field and comments on the visual examination.

Gopalswamy *et al.* (2010) examined the radio-emission characteristics of 222 interplanetary (IP) shocks detected by spacecraft at Sun–Earth L1 using data from multiple satellites (SOHO, Wind, ACE) during Solar Cycle 23 and gave information in a table of 24 columns, specifically the arrival date and time of the shock, the observing spacecraft, the shock speed, the Alfvénic Mach numbers, the ICME type (sheath, ejecta or MC), the ICME time and speed, the CME characteristics (time, CPA, width, speed, acceleration), the associated solar flare (location, duration, size in soft X-rays) and information on the type II burst.

Richardson and Cane (2010) examined a total of 300 ICMEs from the same satellites in addition to IMP 8 and the OMNI database for the years 1996–2009 and gave information

for each event in a table of 18 columns, specifically the arrival time of the shock, the start and the end times of the ICME, the start and the end times of the MC, bidirectional/counterstreaming solar wind suprathermal electron flows (BDEs), bidirectional energetic ion flows (BIFs), the velocities of the ICME and the transit velocity, the Dst minimum *etc.* Further information was added for some events including the most probable CME based on SOHO/LASCO data.

Mitsakou and Moussas (2014) examined 325 ICMEs from the OMNI database for the years 1996–2008 and gave information on the arrival time of the ICME-driven shock, the start and the end times of the ICME and statistical results for the solar wind parameters.

Compared with these studies, the main advantage of the new ICME list is that it provides the full information for each event from its source till the arrival at the Earth. The main findings of the current work are:

- The solar wind data and the magnetic field mean values are at typical interplanetary medium values for some hours before the arrival of the ICME, while the maximum values occur during the sheath of the ICME as a result of the conditions inside the sheath. In the period of the main part of ICMEs the southward component of the magnetic field B_z and the proton density and the proton temperature are at very low levels, similar to the background conditions or typical interplanetary medium values. In particular, the plasma β inside the ICME is much lower than that in the sheath and $\beta < 1$, *i.e.* the magnetic pressure is the dominant factor.
- The transit velocity, calculated in Section 2.3.2, ranges from $\approx 300 \text{ km s}^{-1}$ up to $\approx 2200 \text{ km s}^{-1}$ and the CME linear speed from LASCO ranges from $\approx 90 \text{ km s}^{-1}$ up to 3390 km s^{-1} , with a cross correlation coefficient between these quantities of $r = 0.59$. The transit time for the examined events ranges from 18.5 hours (≈ 0.8 days) up to 136.6 hours (≈ 5.7 days) with a mean value of 62.9 hours (≈ 2.6 days).
- The solar wind speed in the sheath and the solar wind speed in the ICME show a very good correlation with a coefficient equal $r = 0.90$. This result is in accordance with Chi *et al.* (2016).
- During the examined period the Dst index ranges from -422 nT up to $+8 \text{ nT}$ with a mean value of -79 nT , consistent with the mean value of -76 nT obtained from the study of Richardson and Cane (2010), while the southward component of the magnetic field B_z ranges from -78.56 nT up to $+5.41 \text{ nT}$. The minimum value of the southward component of the magnetic field B_z is very well correlated with the Dst minimum values with a correlation coefficient $r = 0.80$. This result is in accordance with the value of the correlation coefficient $r = 0.89$ obtained from the work of Richardson and Cane (2010). The small difference between these results is probably due to the time resolution of the data used by Richardson and Cane (2010): they used 1-hour averaged data of the southward component of magnetic field in the sheath or in the ICME.
- The Ap geomagnetic index ranges from 6 up to 400 for all events with a mean value of 85. The minimum B_z value (in the sheath or in the ICME) and the Ap-index maximum values are highly correlated with $r = 0.84$.
- The linear speed of the CME and the calculated effective acceleration for all examined events have a cross correlation coefficient $r = 0.95$. This value rises to $r = 0.98$ with the exclusion of five points which are out of the 99 % upper or lower prediction levels and are characterized by very high speeds or accelerations. The current research confirms that slow CMEs are accelerated and fast CMEs are generally decelerated. We note that this result is in accordance with the results of Gopalswamy *et al.* (2000).
- For events with $6 \leq \text{Ap} \leq 32$, the Dst minimum value occurs before the Ap maximum value in 33 % of the ICMEs. For strong geomagnetic storms (33 events with $179 \leq \text{Ap} \leq$

400) the Ap maximum is recorded almost ≈ 4 hours before the Dst minimum. For those cases where the Dst index value occurs before the Ap maximum (≈ 4.75 hours before) there are no important geomagnetic effects, except the cases when multiple ICMEs occur in a very short period of hours or 1–2 days, and as a result the initial conditions are already disturbed. Almost half of these events, without important geomagnetic storms, are recorded in the declining phase of Solar Cycle 23 (2005–2009).

- The majority of the geomagnetic storms are due to the ICME main part and not to the sheath, as mentioned in Section 4.1, where $B_{z_ICME} < B_{z_dist}$.
- From a total of 266 CMEs, 209 events (78.6 %) are associated with solar flares, while 57 events (21.4 %) are not associated. Moreover, larger and more energetic solar flares are associated with faster Earth-directed CMEs, resulting in ICMEs which produce intense geomagnetic storms.
- A north–south asymmetry for X-class solar flares is revealed, with 17 events in the northern hemisphere and 30 events in the southern hemisphere. This should be investigated also for the current Solar Cycle 24, for possible association with the changes of the polarity of the solar magnetic field (Hale 22-year cycle).
- For the events which are associated with solar flares in which the magnitude is greater than M1.0 and which are geomagnetic effective producing storms with $Ap \geq 179$, an east–west asymmetry is present, with 6 events in the eastern part of the visible solar disk and 16 events in the western part of the disk.
- The occurrence rate of the ICMEs follows the solar cycle, as found also by other researchers (Chi *et al.*, 2016; Richardson and Cane, 2010; Jian *et al.*, 2006 and references therein) but a contrary effect is found for the ICME characteristics. For example, the maximum values of solar wind plasma and magnetic field parameters are found during the descending phase of the cycle during the years 2003–2006 and not in the period of solar maximum, as was expected. Evidence for a solar-cycle dependence of the fraction of ICMEs that have the characteristics of magnetic clouds is also found. This result is also in accordance with previous works (Chi *et al.*, 2016; Richardson and Cane, 2010; Jian *et al.*, 2006 and references therein).
- The semiannual variation of geomagnetic activity is also found in the current work, confirming the results of previous researchers such as Gonzalez and Tsurutani (1992) and Crooker, Cliver, and Tsurutani (1992). These results imply that the geomagnetic activity depends on the season of the year and in particular the most intense geomagnetic storms occur around the equinoxes.
- Almost 83.5 % of the examined events are associated with fast upstream shocks and from those events 51.4 % are also associated with magnetic clouds (MC type 1 or 2 in our description).

In conclusion we can say that the current work offers, for the first time, all the available information per ICME from its source at the Sun till the arrival at Earth, in one unique list. This list contributes to space weather studies and can be the basis for space weather applications. Specifically, when a new CME identified from the SOHO/LASCO coronagraph, then previous cases of CMEs with the same characteristics, such as linear speed, angular width, possible association with solar flare *etc.* from our catalog, could be used in order to estimate the geomagnetic effects in the case that this CME arrives at Earth.

In a future work, data from this ICME catalog will be the basis for a new CME-index (Paouris, 2013) useful for the study of the cosmic ray intensity modulation over Solar Cycle 23 in a new formula taking into account for the first time the magnetic field, the transit velocity and the angular width of the CME.

This ICME catalog will be extended up to the current Solar Cycle 24 as soon as possible and will be available via the Space Weather Center of the Athens Neutron Monitor Station – A.Ne.Mo.S. (<http://cosray.phys.uoa.gr/index.php/icmes>).

Acknowledgements We are grateful to the providers of the solar, interplanetary, and geomagnetic data used in this work. The coronal mass ejection data are taken from the SOHO/LASCO CME list (http://cdaw.gsfc.nasa.gov/CME_list/). This CME catalog is generated and maintained at the CDaw Data Center by NASA and The Catholic University of America in cooperation with the Naval Research Laboratory. SOHO is a project of international cooperation between ESA and NASA. Thanks are also due to Dr. N. Gopalswamy for useful suggestions and to the anonymous referee for comments improving this paper significantly.

Conflict of interest The authors declare that they have no conflicts of interest.

References

- Andrews, M.D.: 2003, *Solar Phys.* **218**, 261. DOI.
- Bartels, J.: 1932, *Terr. Magn. Atmos. Electr.* **37**, 1. DOI.
- Bochsler, P., Geiss, J., Joos, R.: 1985, *J. Geophys. Res.* **90**, 10779. DOI.
- Borrini, G., Gosling, J.T., Bame, S.J., Feldman, W.C.: 1982, *J. Geophys. Res.* **87**, 7370. DOI.
- Burlaga, L., Sittler, E., Mariani, F., Schwenn, R.: 1981, *J. Geophys. Res.* **86**, 6673. DOI.
- Cane, H.V., Richardson, I.G., St. Cyr, O.C.: 2000, *Geophys. Res. Lett.* **27**, 3591. DOI.
- Chi, Y., Shen, C., Wang, Y., Xu, M., Ye, P., Wang, S.: 2016, *Solar Phys.* **291**, 2419. DOI.
- Chowdhury, P., Kudela, K., Dwivedi, B.N.: 2013, *Solar Phys.* **286**, 577. DOI.
- Cortie, A.L.: 1912, *Mon. Not. Roy. Astron. Soc.* **73**, 52. DOI.
- Crooker, N.U., Cliver, E.W., Tsurutani, B.T.: 1992, *Geophys. Res. Lett.* **19**, 429. DOI.
- Echer, E., Gonzalez, W.D., Tsurutani, B.T., Gonzalez, A.L.C.: 2008, *J. Geophys. Res.* **113**, A05221. DOI.
- Georgoulis, M.K.: 2008, *Geophys. Res. Lett.* **35**, L06S02. DOI.
- Gonzalez, W.D., Tsurutani, B.T.: 1992, In: Svestka, Z., Jackson, B.V., Machado, M.E. (eds.) *Eruptive Solar Flares*, Springer, New York, 277. DOI.
- Gonzalez, W.D., Clua de Gonzalez, A.L., Tsurutani, B.T.: 1993, *Geophys. Res. Lett.* **20**, 1659. DOI.
- Gopalswamy, N.: 2004, In: Poletto, G., Suess, S.T. (eds.) *The Sun and the Heliosphere as an Integrated System 317*, Kluwer, Dordrecht, 201. DOI.
- Gopalswamy, N.: 2006, *J. Astrophys. Astron.* **27**, 243. DOI.
- Gopalswamy, N.: 2009, *Earth Planets Space* **61**, 595. DOI.
- Gopalswamy, N., Yashiro, S., Akiyama, S.: 2007, *J. Geophys. Res.* **112**, A06112. DOI.
- Gopalswamy, N., Lara, A., Lepping, R.P., Kaiser, M.L., Berdichevsky, D., Cyr, O.C.St.: 2000, *Geophys. Res. Lett.* **27**, 145. DOI.
- Gopalswamy, N., Xie, H., Makela, P., Akiyama, S., Yashiro, S., Kaiser, M.L., Howard, R.A., Bougeret, J.-L.: 2010, *Astrophys. J.* **710**, 1111. DOI.
- Gosling, J.T.: 1993, *J. Geophys. Res.* **98**, 18937. DOI.
- Gushchina, R.T., Belov, A.V., Eroshenko, E.A., Obridko, V.N., Paouris, E., Shelting, B.D.: 2014, *Geomagn. Aeron.* **54**, 430. DOI.
- Harrison, R.A.: 1995, *Astron. Astrophys.* **304**, 585.
- Huttunen, K.E.J., Schwenn, R., Bothmer, V., Koskinen, H.E.J.: 2005, *Ann. Geophys.* **23**, 625. DOI.
- Jian, L., Russell, C.T., Luhmann, J.G., Skoug, R.M.: 2006, *Solar Phys.* **239**, 393. DOI.
- Loewe, C.A., Pröls, G.W.: 1997, *J. Geophys. Res.* **102**, 14209. DOI.
- Mavromichalaki, H., Gerontidou, M., Paschalis, P., Papaioannou, A., Paouris, E., Papailiou, M., Souvat-zoglou, G.: 2015, *J. Phys. Conf. Ser.* **632**, 012071. DOI.
- McComas, D.J., Bame, S.J., Barker, P., Feldman, W.C., Phillips, J.L., Riley, P., Griffee, J.W.: 1998, *Space Sci. Rev.* **86**, 563. DOI.
- McIntosh, D.H.: 1959, *Phil. Trans. Roy. Soc. London Ser. A, Math. Phys. Sci.* **251**, 525. DOI.
- McPherron, R.L.: 1999, *Phys. Chem. Earth* **24**, 45. DOI.
- Mitsakou, E., Moussas, X.: 2014, *Solar Phys.* **289**, 3137. DOI.
- Mullan, D.J., Smith, C.W.: 2006, *Solar Phys.* **234**, 325. DOI.
- Newbury, J.A., Russell, C.T., Phillips, J.L., Gary, S.P.: 1998, *J. Geophys. Res.* **105**, 9553. DOI.
- Paouris, E.: 2013, *Solar Phys.* **284**, 589. DOI.
- Paouris, E., Mavromichalaki, H., Belov, A., Gushchina, R., Yanke, V.: 2012, *Solar Phys.* **280**, 255. DOI.

- Papailiou, M., Mavromichalaki, H., Abunina, M., *et al.*: 2013, *Solar Phys.* **283**, 557. [DOI](#).
- Richardson, I.G., Cane, H.V.: 2010, *Solar Phys.* **264**, 189. [DOI](#).
- Russell, C.T., McPherron, R.L.: 1973, *J. Geophys. Res.* **78**, 92. [DOI](#).
- Schwenn, R., Dal Lago, A., Huttunen, E., Gonzalez, W.D.: 2005, *Ann. Geophys.* **23**, 1033. [DOI](#).
- Smith, C.W., Acuna, M.H., Burlaga, L., L'Heureux, J., Ness, N.F., Scheifele, J.: 1998, *Space Sci. Rev.* **86**, 613. [DOI](#).
- Svalgaard, L.: 1977, In: Zirker, J.B. (ed.) *Coronal Holes and High Speed Wind Streams*, Colorado Associated Univ. Press, Boulder, 371.
- Tsurutani, B.T., Gonzalez, W.D.: 1997, In: Tsurutani, B.T., Gonzalez, W.D., Kamide, Y., Arballo, J.K. (eds.) *Magnetic Storms, Geophys. Monogr. Ser.* **98**, AGU, Washington, 77. [DOI](#).
- Vourlidas, A., Buzasi, D., Howard, R.A., Esfandiari, E.: 2002, In: Wilson, A. (ed.) *Solar Variability: From Core to Outer Frontiers SP-506*, ESA, Noordwijk, 91. 92-9092-816-6.
- Wang, Y., Zhang, J.: 2007, *Astrophys. J.* **665**, 1428. [DOI](#).
- Yashiro, S., Gopalswamy, N., Akiyama, S., Michalek, G., Howard, R.A.: 2005, *J. Geophys. Res.* **110**, A12S05. [DOI](#).
- Yermolaev, Yu.I., Lodkina, I.G., Nikolaeva, N.S., Yermolaev, M.Yu.: 2015, *J. Geophys. Res.* **120**, 7094. [DOI](#).
- Zhang, J., Richardson, I.G., Webb, D.F., Gopalswamy, N., Huttunen, E., *et al.*: 2007, *J. Geophys. Res.* **112**, A10102. [DOI](#).